MDPI

Article

Effect of workpiece/tool heat transfer and friction coefficients on accuracy of simulated temperatures and torques in a friction stir welding plunge

Matthew Goodson [1,†], Ryan Melander [2,†], Michael Miles [1,†*] and Troy Munro [1,†]

[1] Brigham Young University Mechanical Engineering Department
[2] Brigham Young University Manufacturing Engineering Department
* Correspondence: mmiles@byu.edu
† These authors contributed equally to this work.

Abstract: Friction stir process models are typically validated by tuning heat transfer and friction coefficients until measured temperatures in either tool or workpiece, but rarely both, match simulated results. A three-dimensional finite element model for a tool plunge in AA6061-T6 is validated for temperature predictions in both tool and workpiece, using a friction coefficient that varies with time. Peak workpiece temperatures were within 1.5% of experimental temperatures and tool temperatures were off by 80 °C. Sensitivity of predicted temperatures on the workpiece/tool heat transfer coefficient is shown to be high for the tool and low for the workpiece, while spindle torque is slightly underpredicted in the best case. These results show that workpiece/tool interface properties must be tuned by considering predictions on both sides of the heat generation interface in order to ensure a reliable process simulation.

Keywords: finite element models; friction stir welding; workpiece/tool interfacial heat transfer coefficient; friction coefficient

Citation: Goodson, M.; Melander, R.; Michael, M.; Munro, T. Effect of workpiece/tool heat transfer and friction coefficients on accuracy of simulated temperatures and torques in a friction stir welding plunge. *Journal Not Specified* **2023**, *1*, 0. https://doi.org/

Received:
Revised:
Accepted:
Published:

1. Introduction

Friction Stir Welding (FSW) is a solid-state joining process with advantages over common fusion welding approaches. The process involves a rapidly rotating tool with a pin that is plunged into the parts to be welded, a dwell phase to increase heat, and then a traverse phase along the joint to create a weld. The plunge process is shown in Figure 1 and exhibits many of the extreme thermomechanical processes that are characteristic of FSW. Since the welding temperatures remain below the melting point of the material, the physical properties of the weld are often better than those associated with fusion welding [1]. FSW has been used to weld aluminum, copper, and dissimilar metals, which are typically unweldable using fusion-based processes [2]. With these advantages, FSW has seen widespread adoption in the automotive, aerospace, and rail transportation industries [3].

Since the invention of FSW in 1991 [4], experimental efforts have developed the process into a viable approach for many applications, but these development efforts are typically trial-and-error based. Models of the FSW process began to appear in the early 2000s [5–12], in an effort to better understand the physics of the process and to speed up its development for industrial applications. These models are typically validated against experimental data, with various levels of rigor. However, the model inputs are not always measured independently from the model development and are simply adjusted to align simulation predictions with experiments.

The two most cited papers in the FSW heat transfer modeling space are from Chao and Khandkar, both of whom used thermocouples for validation measurements. Chao, et al. [6] employed nine thermocouples in the AA 2195 workpiece at different distances from the weld center-line and five thermocouples attached to the M2 steel tool at varied distances

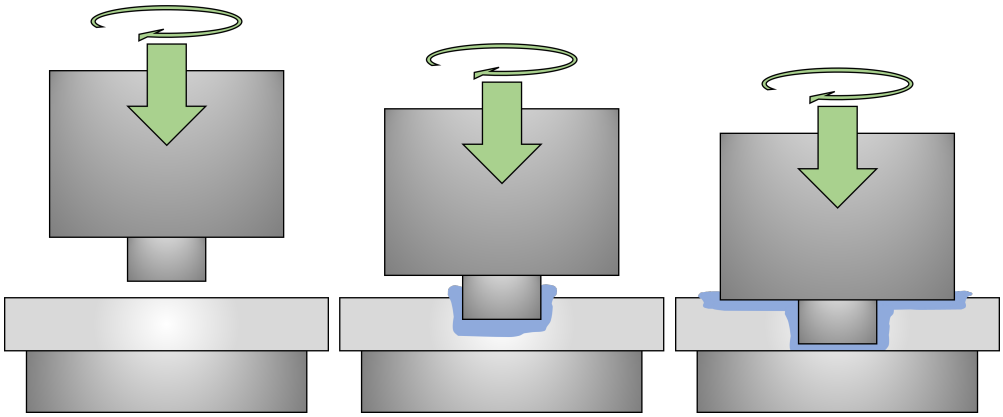

Figure 1. Schematic showing the plunge step of FSW, where the pin engages the workpiece, and finally, where the shoulder is plunged into the material.

above the shoulder. Commercial finite element codes, ABAQUS and WELDSIM, were used to model the steady-state heat transfer of the tool and the transient heat transfer of the workpiece, respectively. A good match was made between experimental and simulation temperature profiles by fitting the heat input to the workpiece and to the tool. The tool and workpiece were modeled separately, and in each case, the heat input was the fitting variable but with no reference to a physical law. Khandkar, et al. [9] also matched an experiment with a model, where a moving heat input was used as a boundary condition. 25 thermocouples were embedded in the AA 6061-T651 workpiece to measure temperature during the experiment. Good agreement was found between experiment and model predictions. The heat transfer coefficient at the work- piece/backing plate interface ($h_{W/B}$) was varied to study its effect on results and to find a good match. A value of $h_{W/B}$ = 1,000 W m^{-2} K^{-1} provided the best result. The tool and the workpiece were modeled but validation of the model temperatures was only performed on the workpiece. The model relates heat generation to physical laws, which is an improvement on previous models.

Temperature measurements in the workpiece are the most common method to validate models [3,13–18]. Andrade, et al. [19] fitted model workpiece temperature profiles to hundreds of experiments done in aluminum to determine trends in torque and workpiece temperatures based on geometry and welding parameter inputs. Fewer papers use temperature measurements in the tool to validate models [2]. Nakamura, et al. [20] was focused on matching simulation tool temperatures to experiments and found that $h_{W/B}$ = 2,000 W m^{-2} K^{-1} provided the best agreement with experiment of AA 6061-T6 workpiece on an undefined backing plate. Danesh, et al. [21] validated a model using both tool and workpiece temperature measurements, but provides no information on the interfacial condition between the tool and workpiece other than defining the heat generation.

Accurately defining boundary conditions is important for having a robust model. The three heat transfer interactions when modeling FSW are the following: the heat transfer between the tool or workpiece and the environment ($h_{W/A}$), the heat transfer between the workpiece and the backing plate ($h_{W/B}$), and the heat transfer between the workpiece and the tool ($h_{W/T}$). Figure 2 shows the variation in the literature for these three heat transfer coefficients. Of the three, the heat transfer coefficient at the workpiece/tool interface, $h_{W/T}$, has not been measured directly via experiment and is thus a parameter that is adjusted to tune model results [22]. If a measurement of $h_{W/T}$ could be conducted, then the only remaining fitting parameter would be the friction coefficient. However, the sensitivity of workpiece and tool temperatures to variations in $h_{W/T}$ needs to be understood prior to designing such experiments.

Despite the models and simulations that have been developed and the advances in accuracy and understanding of the physics behind FSW, we have not seen models in the literature that were validated simultaneously in both the workpiece and the tool. This calls into question whether the heat generation at the workpiece/tool interface was accurately

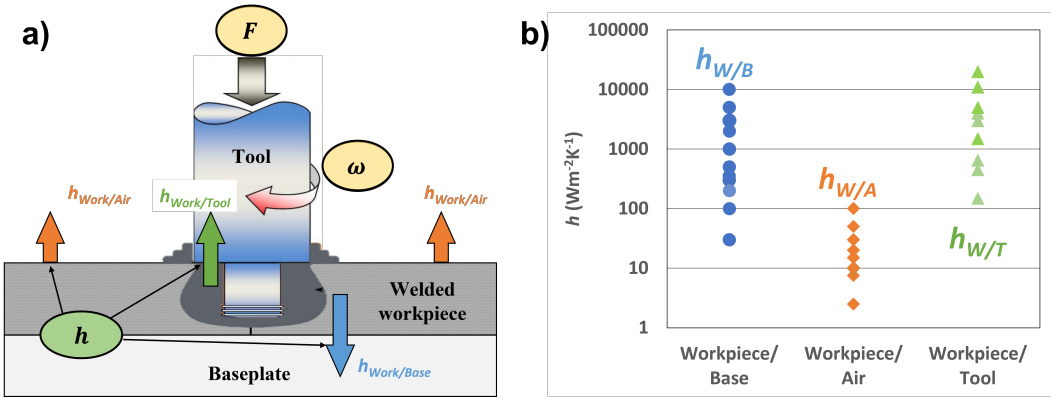

Figure 2. (a) Interfaces in a FSW model whereby the different h values must be specified, and (b) the range of heat transfer coefficient values that have been used over the last 20 years [23]. Copyright 2021, Springer Nature.

simulated, as it is fairly straightforward to tune a model in order to match temperatures for one side of the interface. This paper presents a model of the plunge phase of FSW where both tool and work-piece temperatures were modeled and validated by experiment. The effect of varying the heat transfer coefficient between the workpiece and the tool, $h_{W/T}$, on predicted temperatures will be discussed. The role of friction levels in achieving a good agreement between simulation and experiment will also be considered.

2. Methods

2.1. Experimental procedure

The plunge phase of FSW was carried out experimentally on AA 6061-T6 plates using a tool made of H13 steel. The machine used for the experiments is a TTI High Stiffness RM2 FSW machine. A Bond Technologies B&R-based programmable logic controller with high-speed data acquisition and control was used to program the welding parameters [24]. The machine controls rotation speed, tool displacement, and force. The FSW machine holds the tool and a Bluetooth collar for relaying thermocouple data [25], see Figure 3. Thermocouple data was recorded in the tool and workpiece; for full experiment description see, Table S1, and Fig. S1 in Section S1.1.

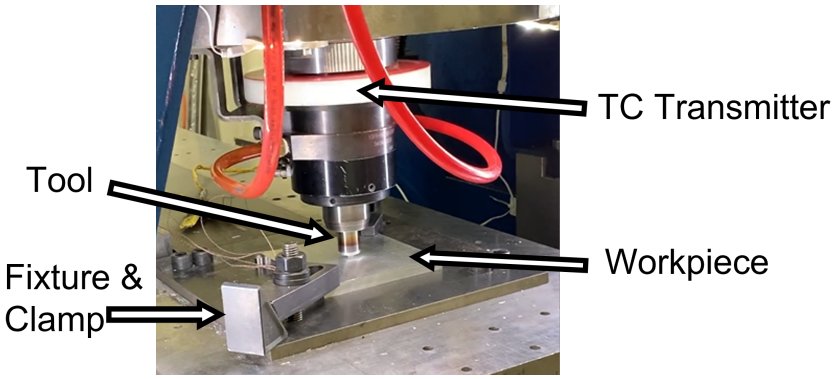

Figure 3. FSW plunge experiment system, including TC instrumentation and fixtures.

2.2. Numerical modeling

The model is developed using the ForgeNxt software [26], which has the ability to simulate large strain, thermo-mechanical processes. An isotropic, viscoplastic Norton-Hoff law is used to model the evolution of material flow stress as a function of strain, strain rate, and temperature, see Figure 4. The expression for the deviatoric stress tensor, s, is shown below:

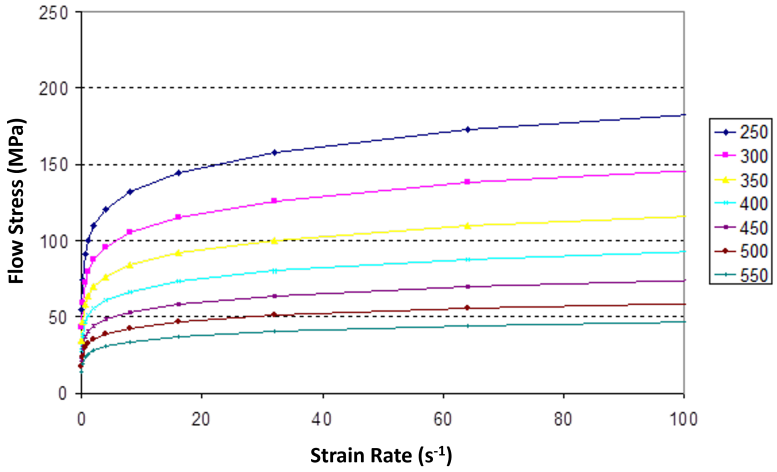

Figure 4. Temperature dependent flow stress values for aluminum used in the model, temperature in °C.

$$s = 2K(\sqrt{3}\dot{\bar{\epsilon}})^{m-1}\dot{\epsilon} \tag{1}$$

where $\dot{\epsilon}$ is the strain rate tensor, $\dot{\bar{\epsilon}}$ is the effective strain rate, K is the material consistency, and m is the strain rate sensitivity. K (Eq. 2) is a function of temperature T and equivalent strain $\bar{\epsilon}$, where n is the strain hardening exponent and β is a thermal softening parameter, and ϵ_0 is the prestrain term:

$$K = K_0(\epsilon_0 + \bar{\epsilon})^n e^{\frac{\beta}{T}} \tag{2}$$

This viscoplastic law is capable of modeling material flow stresses in the region of the weld, while providing the contact stresses with the tool that are used to calculate the friction shear stress at the workpiece/tool interface.

Friction at the workpiece/tool interface is modeled using Norton's viscoplastic law, which simulates the shearing of a boundary layer of workpiece material in order to calculate the shear stress at the workpiece/tool interface:

$$\tau(v) = -\alpha K|\Delta v_s|^{p_f - 1}\Delta v_s \tag{3}$$

where α is the viscoplastic friction coefficient, K is seen previously in Equation 2, Δv_s is the relative sliding velocity at the workpiece/tool interface, and p_f is the sensitivity to sliding velocity, which is equivalent to the strain rate sensitivity for the workpiece material [27].

Heat generated by plastic deformation is modeled by the following term:

$$\dot{q}_v = f\bar{\sigma}\dot{\bar{\epsilon}} \tag{4}$$

where $\bar{\sigma} = \sqrt{\frac{3}{2}s : s}$ is the equivalent stress, and the factor f takes into account the fraction of energy converted into heat, taken as 0.9 in this paper [28]. Heat generation from friction at the workpiece/tool interface is given by:

$$\dot{q}_f = \tau \cdot \Delta v_s \tag{5}$$

where τ is the friction shear stress given by Equations 3. Frictional heat is shared between the workpiece and tool as a function of the effusivities of each, where the material with higher effusivity receives a greater proportion of the frictional heat. Effusivity is defined as $\sqrt{\rho c k}$, where ρ is density, c is heat capacity, and k is thermal conductivity; for further model description, see Fig. S2, Fig. S3, Fig. S4, and Table S2 in Section S1.2.

2.2.1. FSW Plunge Model

Boundary conditions and sensor locations are set to complete the model. The various values for the heat transfer coefficients and friction coefficients are referenced from literature values or determined by tuning of the model. Figure 5 shows the sensor locations and boundary conditions with the following parameters:

1. $h_{W/T} = 10, 20, 30, 40, 50$ kW m^{-2} K^{-1} (40 kW m^{-2} K^{-1} used for temperature matching)
2. $h_{T/A} = h_{W/A} = 10$ W m^{-2} K^{-1} [20]
3. $h_{W/B} = 500$ W m^{-2} K^{-1} [15]
4. α = s-curve, Norton's viscoplastic law (see Fig. S6)
5. $h_{T/holder}$ = adiabatic
6. $T_\infty = 28°C$

Some simplifications are made with the geometry and boundary conditions between the tool and the tool holder; for full justification, see Section S1.3.

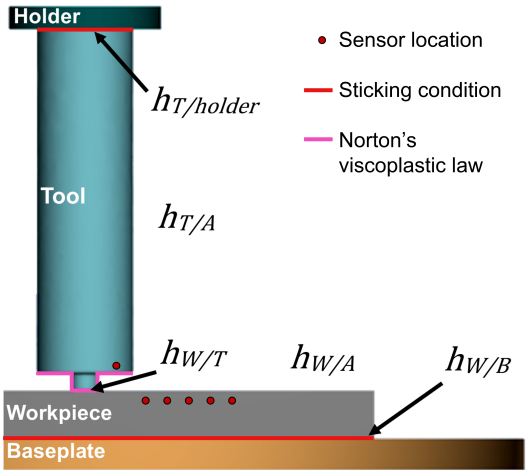

Figure 5. Schematic detailing the location of the different thermal boundary conditions and frictional boundary conditions. The baseplate and holder are set at a constant temperature of 20 °C.

The tool is meshed with 116339 elements and the workpiece is meshed with 49547, with increased mesh density in regions expected to experience high strain rate and temperature gradients. Given the high strains in the portions of the workpiece under the tool, zones are defined for remeshing, which is necessary to avoid element distortion. High mesh densities are maintained in these zones, capturing the high strain rate and temperature gradients inherent in the process.

3. Analysis/Results

3.1. 3D model temperature and torque validation

Validation of the 3D model is accomplished by comparing temperature data at the same locations as the thermocouples in an experiment. Besides the thermal histories in the workpiece, the tool temperature is also recorded, along with the tool's vertical displacement and both spindle loads and torques. Difficulty arises in matching all these parameters accurately because of the highly coupled processes involved in the FSW process. For example, there is not a one-to-one relationship between changing an input parameter and the output. Previous models in the literature have dealt with these difficulties by limiting model fitting based solely on either tool or workpiece temperature [9,13–15,20]. The current work has attempted to develop a model that can predict all these parameters simultaneously, compared to previous work where these effects are often studied separately.

Figure 6 shows the result of tuning the friction curve such that the simulated temperatures match the experimental thermocouple data. A region of error due to thermocouple positioning that overlaps many of the experimental markers is included, meaning that the

simulated data is within the calculated error of the experimental data, (see Section S2 for fitting process and Fig. S6 for TC error explanation). Also, the percent differences between peak experimental temperatures and peak simulated temperatures is less than 1.5% for all sensor locations.

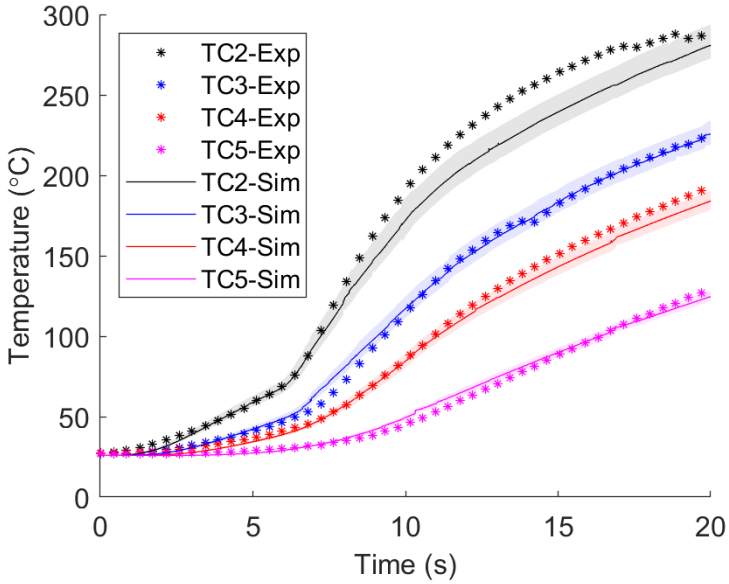

Figure 6. Resulting temperatures within the workpiece after tuning of the friction curve (see, Fig. S6). Markers represent measurements at each position and simulation data is represented by a solid line with a shaded error region around the line that accounts for possible error in thermocouple positioning.

The torque from the simulation is calculated and compared to experiment to validate mechanical performance. The following equation is used to estimate the simulation torque:

$$\begin{aligned} P &= T\omega \\ P &= \frac{\pi}{30} T N_{rpm} \end{aligned} \tag{6}$$

where P is power in watts, T is torque in N-m, and ω is the rotational velocity in rad s^{-1}. Equation 6 is simplified for rotational velocity in rpm where N_{rpm} is the number of rotations per minute of the tool. Torque measurements from the experiment are acquired from the FSW machine and power outputs from the simulation are converted to torque using Equation 6. The torque from the simulation matches the experiment quite well, as seen in Figure 7. The peak torques are very similar, while the quasi steady-state portion of the curve is somewhat underestimated in the simulation. Additionally, the steep increase in torque at 7 seconds when the tool shoulder engages the workpiece is also captured by the simulation, although the simulation has a steeper slope. Torque is a good indicator of simulation accuracy, as it incorporates material behavior as well as interface behavior, in terms of how friction resists the rotation of the tool.

3.2. Sensitivity of temperatures to $h_{W/T}$

Having validated the model, the next step is to vary the values of $h_{W/T}$ while maintaining the tuned values of the friction coefficient. This is done to determine the effect of $h_{W/T}$ on the workpiece and tool temperatures. Values of $h_{W/T}$ used for the simulation were 10, 20, 30, 40, and 50 kW m^{-2} K^{-1}, based on the higher range of values in the literature (Figure 2). Figure 8 shows how the different values of $h_{W/T}$ affect the temperature in the workpiece. As the value of $h_{W/T}$ increases, there is a negligible affect on the peak temperature, (see Fig. S8). The high k of the aluminum facilitates the transfer of heat from the interface to

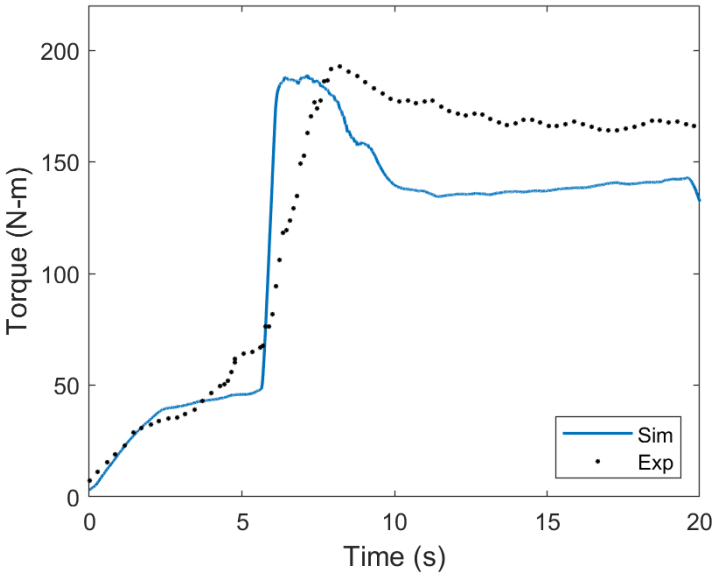

Figure 7. Simulated and experimental torque from FSW plunge. The simulated values are smoothed with a running average.

the boundaries of the workpiece at a sufficiently high rate that changes in $h_{W/T}$ lead to minimal temperature changes in the workpiece. This result has the potential to be different for less thermally conductive materials such as stainless steel.

In addition to the workpiece, the effect of $h_{W/T}$ on tool temperature is also studied, where variation in $h_{W/T}$ had a noticeable effect. Figure 9 shows that as $h_{W/T}$ decreases, the temperature in the tool shoulder increases, (also see Fig. S8). Also, as $h_{W/T}$ increases the peak temperature in the tool decreases. The lower k of the H13 tool steel, relative to the aluminum workpiece, results in the build up of heat close to the interface where heat is generated. As $h_{W/T}$ decreases, less heat is conducted from the hotter tool to the cooler workpiece, thus further contributing to greater tool temperatures. This results in a higher temperature gradient, resulting in a higher temperature near the interface, where the thermocouple sensor is located. There is likely a threshold value where further increasing $h_{W/T}$ no longer decreases the peak temperature in the tool, as seen with $h_{W/T}$ values equal to 40 and 50 kW m^{-2} K^{-1}. The difference between 50 and 10 kW m^{-2} K^{-1}, as shown in Figure 9, is around 140 °C with the difference in peak temperature increasing each time $h_{W/T}$ decreases by 10 kW m^{-2} K^{-1}. There is a difference of about 80 °C between the experimental tool temperature and the simulated temperatures at $h_{W/T}$ = 40, 50 kW m^{-2} K^{-1}. This is the result of first matching the workpiece temperatures while having the secondary objective of matching the tool temperatures.

The discrepancy between experiment and simulation in the case of tool temperature could be related to the sharing of frictional heat at the interface, which is partitioned based on the effusivities of the materials in contact. As such, the physical parameters of both the AA6061 and the H13 materials are confirmed through several publicly available sources [29]. However, if these values are not accurate for the full range of temperatures that occurred during the plunge, then the sharing of heat could be a source of error in the simulation. The challenge of predicting tool temperatures in this case highlights why it is critical to validate a FSW welding model with measurements on both sides of the heat generation interface. It is relatively straightforward to match temperatures in either the tool or workpiece via model tuning, but far more difficult to match in both tool and workpiece, while also achieving a reasonable prediction for spindle torque.

To visualize the effect of $h_{W/T}$ on both the tool and the workpiece simultaneously, Figure 10 compares the thermal gradients at the final time step of the simulation for all

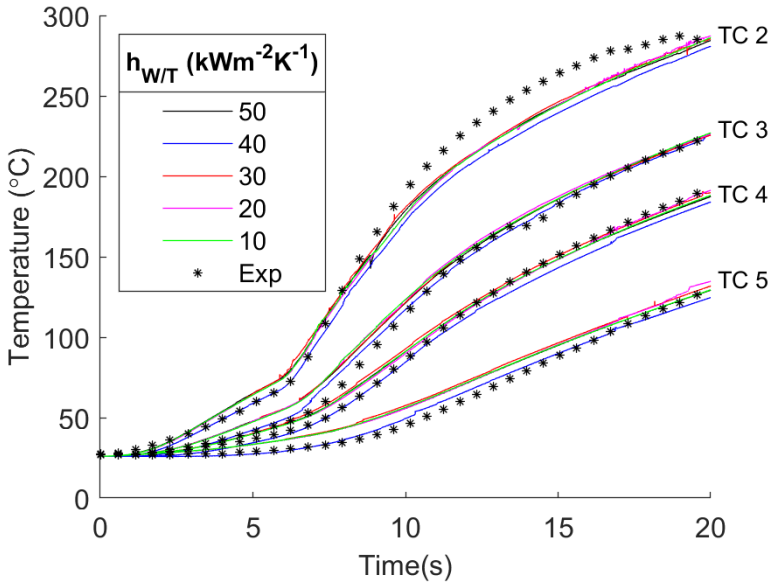

Figure 8. Results of different $h_{W/T}$ values for workpiece temperature plotted with the experimental values for comparison. For each value of $h_{W/T}$ there are four sets of lines plotted, one for each thermocouple location.

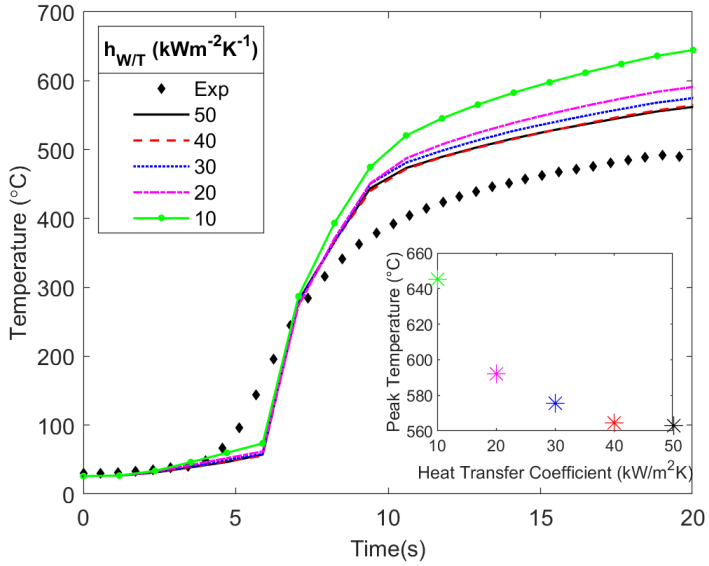

Figure 9. Effect of varying $h_{W/T}$ on tool temperature compared with the experimental results. A difference of about 140 °C is observed between simulations when the lowest and highest $h_{W/T}$ values are used.

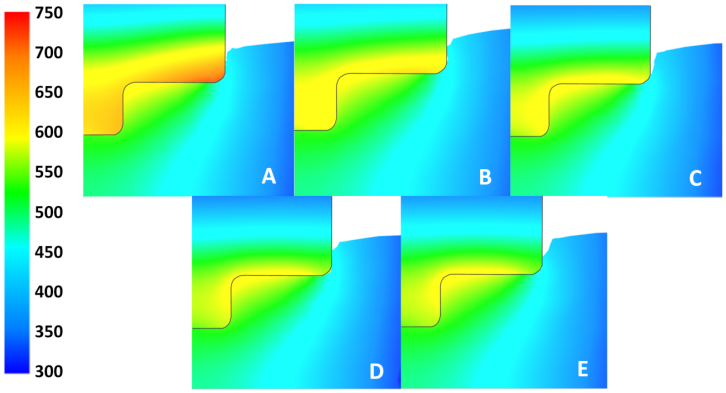

Figure 10. Thermal plots of the tool and workpiece (one half of section view) for each simulated value of $h_{W/T}$ at 20 seconds. Plots A through E represent $h_{W/T}$ values of 10, 20, 30, 40, and 50 kW m^{-2} K^{-1} respectively. Temperature scale is in units of °C.

values of $h_{W/T}$. From Figures 8 and 10, it is evident that the various $h_{W/T}$ values have a negligible effect on workpiece temperature at the thermocouple sensor locations as well as a negligible effect on the overall thermal gradient in the workpiece. However, Figures 8 and 10, show that $h_{W/T}$ does affect the tool temperature at the thermocouple sensor location and the overall thermal gradient differs between $h_{W/T}$ values. For $h_{W/T}$ = 10 kW m^{-2} K^{-1}, more heat builds up in the tool near the interface because it is not able to conduct across the interface as easily compared to $h_{W/T}$ = 50 kW m^{-2} K^{-1}. Heat buildup does not occur in the workpiece because of the greater k and diffusivity of the aluminum workpiece.

4. Discussion

The current modeling results show that $h_{W/T}$ values less than 10 kW m^{-2} K^{-1} are under-representing the heat transfer between the tool and the workpiece. Nakamura [20] employed a value of $h_{W/T}$ = 5 kW m^{-2} K^{-1}, showing a good match with tool temperature measurements, but no measurement in the workpiece is done and therefore it is difficult to know how the model did in predicting workpiece temperatures. Our results show lower $h_{W/T}$ values provide tool temperatures well above those measured during the experiment. A greater value for $h_{W/T}$ is more likely to be the case, due to the high pressures and intimate contact between the tool and workpiece that is facilitated by intense shearing of the material, compared to other models that predict thermal contact conductance with similar pressure but under static conditions [30]. Also, a higher $h_{W/T}$ better matches the tool temperature as shown in Figures 9.

The results from this study are only of the transient plunge step of the FSW process. Therefore, comparisons between this and other works for steady state models are not directly applicable. Steady state models use a fixed friction coefficient for a transverse weld process whereas a changing friction coefficient was used to adjust for the transient nature of the plunge process [2,20]. However, the current results can be compared to other works that have studied the plunge process [31–33]. Figure 10 agrees with work done by Yu et al. [34] showing similar thermal contours in the workpiece with the hottest location near the root of the tool and a similar thermal gradient moving out into the workpiece.

A possible source of error is the material properties of the model. These properties evolve with temperature and are only as accurate as the reference used for the simulation [29]. If these temperature dependent properties are inaccurate, then the effusivity values for workpiece and tool, used to partition heat generated at the contact interface between them, would be affected. For explanation on other model limitations, see Section S3.

Modeling of both the tool and workpiece should become a common practice in validating a FSW model. Doing so will help to increase accuracy of model predictions by ensuring that heat generation at the workpiece/tool interface, and the interactions that take place across the boundary, are correct. If only the tool or the workpiece is modeled

and validated, then these interactions cannot be evaluated rigorously. Validating the model on both sides of the workpiece/tool contact interface serves to highlight where model predictions are lacking and points to a need for understanding nuanced phenomena like how the heat generated by the tool is partitioned across the interface. This work also points to the need for independent determination of friction law parameters and heat transfer coefficients in order to render FSW models more robust and to improve their predictions against experiments.

5. Conclusions

Accurate modeling of FSW requires rigorous model validation, which should be done for both the tool and the workpiece. Model development requires tuning some parameters in order to match experimental results. The process parameters are highly coupled, which means parameter changes do not always have a predictable outcome. Normally the workpiece temperatures are of the greatest interest because the resulting weld quality and properties are of value for FSW process development. For this reason, the model tuning simulations detailed here have been primarily focused on matching the workpiece temperatures. However, the model development also aimed to match tool temperature, which led to using more accurate physical parameters to improve partitioning of heat at the tool/workpiece interface. Further work on developing friction law parameters independent of model tuning, via experiments, will lead to more predictable and robust models. At the present time, a validation approach where both workpiece and tool results are matched with experiments via parameter tuning should lead to more accurate modeling than most prior efforts where partial validation has been typical.

Based on the results of the current work, the following conclusions are made:

1. A time dependent friction coefficient provides accurate model predictions of the workpiece temperatures.
2. Decreasing the value of $h_{W/T}$ showed no noticeable change in workpiece temperatures, as the high thermal conductivity of AA6061-T6 dissipates heat quickly. For a less thermally conductive workpiece, such as stainless steel or titanium, variations in $h_{W/T}$ would likely have a larger impact on the temperatures within the workpiece.
3. Decreasing the value of $h_{W/T}$ results in higher tool temperatures, as this lowers the amount of heat transferring across the contact interface to the workpiece.
4. Validation of model temperature predictions must be done on both sides of the workpiece/tool interface in order to achieve reasonable results. The model shows that partitioning of heat from friction at this interface strongly influences temperature predictions, and is dependent on accurate physical parameter data. Therefore, the typical validation approach of matching temperatures in just the tool, or just the workpiece, will not lead to a predictive model.

Author Contributions: Matthew Goodson: Conceptualization, Methodology, Software, Validation, Formal analysis, Investigation, Data Curation, Writing – Original Draft, Writing – Review & Editing, Visualization, Project administration Ryan Melander: Methodology, Software, Validation, Formal analysis, Investigation, Data Curation, Writing – Original Draft, Writing – Review & Editing, Visualization Michael Miles: Conceptualization, Software, Resources, Writing – Original Draft, Writing – Review & Editing, Resources, Supervision, Funding acquisition, Project administration Troy Munro: Conceptualization, Writing – Review & Editing, Supervision, Funding acquisition, Resources, Project administration

Funding: This work was supported by the National Science Foundation under Grant No. 1935767.

Institutional Review Board Statement: Not applicable.

Informed Consent Statement: Not applicable.

Data Availability Statement: Data is contained within the article or supplementary material or can be requested.

Conflicts of Interest: The authors declare no conflict of interest.

The following abbreviations are used in this manuscript:

References

1. Hwang, Y.M.; Kang, Z.W.; Chiou, Y.C.; Hsu, H.H. Experimental study on temperature distributions within the workpiece during friction stir welding of aluminum alloys. *International Journal of Machine Tools and Manufacture* **2008**, *48*, 778–787. https://doi.org/10.1016/j.ijmachtools.2007.12.003.
2. Assidi, M.; Fourment, L.; Guerdoux, S.; Nelson, T. Friction model for friction stir welding process simulation: Calibrations from welding experiments. *International Journal of Machine Tools and Manufacture* **2010**, *50*, 143–155. https://doi.org/10.1016/j.ijmachtools.2009.11.008.
3. Bachmann, M.; Carstensen, J.; Bergmann, L.; dos Santos, J.F.; Wu, C.S.; Rethmeier, M. Numerical simulation of thermally induced residual stresses in friction stir welding of aluminum alloy 2024-T3 at different welding speeds. *The International Journal of Advanced Manufacturing Technology* **2017**, *91*, 1443–1452. https://doi.org/10.1007/s00170-016-9793-8.
4. Thomas, W.M. Friction stir butt welding. *Int. Patent No. PCT/GB92/02203* **1991**.
5. Ulysse, P. Three-dimensional modeling of the friction stir-welding process. *International Journal of Machine Tools and Manufacture* **2002**, *42*, 1549–1557. https://doi.org/10.1016/S0890-6955(02)00114-1.
6. Chao, Y.J.; Qi, X.; Tang, W. Heat transfer in friction stir welding - Experimental and numerical studies. *Journal of Manufacturing Science and Engineering, Transactions of the ASME* **2003**, *125*, 138–145. https://doi.org/10.1115/1.1537741.
7. Chen, C.M.; Kovacevic, R. Finite element modeling of friction stir welding—thermal and thermomechanical analysis. *International Journal of Machine Tools and Manufacture* **2003**, *43*, 1319–1326. https://doi.org/10.1016/S0890-6955(03)00158-5.
8. Song, M.; Kovacevic, R. Thermal modeling of friction stir welding in a moving coordinate system and its validation. *International Journal of Machine Tools and Manufacture* **2003**, *43*, 605–615. https://doi.org/10.1016/S0890-6955(03)00022-1.
9. Khandkar, M.Z.H.; Khan, J.A.; Reynolds, A.P. Prediction of temperature distribution and thermal history during friction stir welding: input torque based model. *Science and Technology of Welding and Joining* **2003**, *8*, 165–174. https://doi.org/10.1179/136217103225010943.
10. Colegrove, P.A.; Shercliff, H.R. Experimental and numerical analysis of aluminium alloy 7075-T7351 friction stir welds. *Science and Technology of Welding and Joining* **2003**, *8*, 360–368. https://doi.org/10.1179/136217103225005534.
11. Schmidt, H.; Hattel, J. A local model for the thermomechanical conditions in friction stir welding. *Modelling and Simulation in Materials Science and Engineering* **2004**, *13*, 77–93. https://doi.org/10.1088/0965-0393/13/1/006.
12. Soundararajan, V.; Zekovic, S.; Kovacevic, R. Thermo-mechanical model with adaptive boundary conditions for friction stir welding of Al 6061. *International Journal of Machine Tools and Manufacture* **2005**, *45*, 1577–1587. https://doi.org/10.1016/j.ijmachtools.2005.02.008.
13. Ghetiya, N.D.; Patel, K.M.; Patel, A.B. Prediction of temperature at weldline in air and immersed friction stir welding and its experimental validation. *The International Journal of Advanced Manufacturing Technology* **2015**, *79*, 1239–1246. https://doi.org/10.1007/s00170-015-6906-8.
14. Contuzzi, N.; Campanelli, S.L.; Casalino, G.; Ludovico, A.D. On the role of the Thermal Contact Conductance during the Friction Stir Welding of an AA5754-H111 butt joint. *Applied Thermal Engineering* **2016**, *104*, 263–273. https://doi.org/10.1016/j.applthermaleng.2016.05.071.
15. Paulo, R.M.F.; Carlone, P.; Paradiso, V.; Valente, R.A.F.; Teixeira-Dias, F. Prediction of friction stir welding effects on AA2024-T3 plates and stiffened panels using a shell-based finite element model. *Thin-Walled Structures* **2017**, *120*, 297–306. https://doi.org/10.1016/j.tws.2017.09.009.
16. Chen, G.; Li, H.; Wang, G.; Guo, Z.; Zhang, S.; Dai, Q.; Wang, X.; Zhang, G.; Shi, Q. Effects of pin thread on the in-process material flow behavior during friction stir welding: A computational fluid dynamics study. *International Journal of Machine Tools and Manufacture* **2018**, *124*, 12–21. https://doi.org/10.1016/j.ijmachtools.2017.09.002.
17. Costa, M.I.; Leitão, C.; Rodrigues, D.M. Parametric study of friction stir welding induced distortion in thin aluminium alloy plates: A coupled numerical and experimental analysis. *Thin-Walled Structures* **2019**, *134*, 268–276. https://doi.org/10.1016/j.tws.2018.10.027.
18. Verma, S.; Misra, J.P.; Gupta, M. Study of Temperature Distribution During FSW of Aviation Grade AA6082. Springer, 2019, pp. 185–202. https://doi.org/10.1007/978-981-13-6287-3_13.
19. Andrade, D.G.; Leitão, C.; Dialami, N.; Chiumenti, M.; Rodrigues, D.M. Modelling torque and temperature in friction stir welding of aluminium alloys. *International Journal of Mechanical Sciences* **2020**, *182*. https://doi.org/10.1016/j.ijmecsci.2020.105725.
20. Nakamura, T.; Obikawa, T.; Yukutake, E.; Ueda, S.; Nishizaki, I. Tool Temperature and Process Modeling of Friction Stir Welding. *Modern Mechanical Engineering* **2018**, *08*, 78–94. https://doi.org/10.4236/mme.2018.81006.
21. Babu, S.D.D.; Sevvel, P.; Kumar, R.S.; Vijayan, V.; Subramani, J. Development of Thermo Mechanical Model for Prediction of Temperature Diffusion in Different FSW Tool Pin Geometries During Joining of AZ80A Mg Alloys. *Journal of Inorganic and Organometallic Polymers and Materials* **2021**, *31*, 3196–3212. https://doi.org/10.1007/s10904-021-01931-4.
22. Akbari, M.; Asadi, P.; Sadowski, T. A Review on Friction Stir Welding/Processing: Numerical Modeling. *Materials* **2023**, *16*, 5890. https://doi.org/10.3390/ma16175890.

23. Ellis, D.; Goodson, M.; Miles, M.; Munro, T. Optimized Design for a Device to Measure Thermal Contact Conductance During Friction Stir Welding. *International Journal of Thermophysics* **2020**, *42*, 6. https://doi.org/10.1007/s10765-020-02746-0.
24. Taysom, B.S.; Sorensen, C.D. Advances in Signal Processing for Friction Stir Welding Temperature Control. Springer International Publishing, 2019, pp. 135–147. https://doi.org/10.1007/978-3-030-05752-7_13.
25. Wright, A.; Munro, T.R.; Hovanski, Y. Evaluating temperature control in friction stir welding for industrial applications. *Journal of Manufacturing and Materials Processing* **2021**, *5*. https://doi.org/10.3390/jmmp5040124.
26. Transvalor. FORGE NxT simulation software.
27. Murillo-Marrodan, A.; Garcia, E.; Cortes, F. A study of friction model performance in a skew rolling process numerical simulation. *International Journal of Simulation Modelling* **2018**, *17*, 569–582. https://doi.org/10.2507/IJSIMM17(4)441.
28. Al-Badour, F.; Merah, N.; Shuaib, A.; Bazoune, A. Coupled Eulerian Lagrangian finite element modeling of friction stir welding processes. *Journal of Materials Processing Technology* **2013**, *213*, 1433–1439. https://doi.org/10.1016/j.jmatprotec.2013.02.014.
29. Ltd., S.S. JMatPro, 2014.
30. Bahrami, M.; Culham, J.; Yovanovich, M. Modeling thermal contact resistance: a scale analysis approach. *J. Heat Transfer* **2004**, *126*, 896–905.
31. Iqbal, M.P.; Jain, R.; Pal, S.K. Numerical and experimental study on friction stir welding of aluminum alloy pipe. *Journal of Materials Processing Technology* **2019**, *274*, 116258. https://doi.org/10.1016/j.jmatprotec.2019.116258.
32. Perović, M.; Veljić, D.; Rakin, M.; Radović, N.; Sedmak, A.; Bajić, N. Friction-stir welding of high-strength aluminium alloys and a numerical simulation of the plunge stage. *Materiali in Tehnologije* **2012**, *46*, 215–221. Accepted: 2021-03-10T11:43:00Z Publisher: Institute of Metals and Technology.
33. Jabbari, M. Effect of the Preheating Temperature on Process Time in Friction Stir Welding of Al 6061-T6. *Journal of Engineering* **2013**, *2013*, e580805. Publisher: Hindawi, https://doi.org/10.1155/2013/580805.
34. Yu, M.; Li, W.Y.; Li, J.L.; Chao, Y.J. Modelling of entire friction stir welding process by explicit finite element method. *Materials Science and Technology* **2012**, *28*, 812–817. https://doi.org/10.1179/1743284711Y.0000000087.

S1 Methods

S1.1 Experimental procedure

All tests are force controlled with different tool rpm as seen in Table S1.

The AA 6061-T6 workpieces each have dimensions of $L \times W \times H$ = 152.4 × 152.4 × 12.7 mm, with type K thermocouples at locations shown in Fig. S1a. Placement of thermocouples directly under the tool in the workpiece is avoided to limit thermocouple movement during the plunge. The thermocouple locations are chosen to capture the thermal gradients that occur during a non-steady-state plunge, where temperatures vary spatially and temporally over a short period of time.

The tool has a shoulder diameter of 25.3 mm, body length from the top of tool to the shoulder of 90.7 mm, and a flat shoulder. The tool has an unthreaded straight pin with a diameter of 7.1 mm and a length of 4.5 mm. The tool is also prepared with type K thermocouples placed 1 mm above the tool surface in the center of the pin and in the shoulder, with locations shown in Fig. S1b.

Table S1: Force and rotational speed of test groups

Test #	kN	rpm
1	27	400
2	27	600
3	36	400
4	36	600

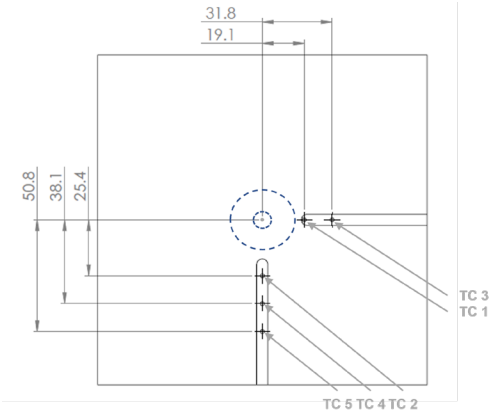

(a)

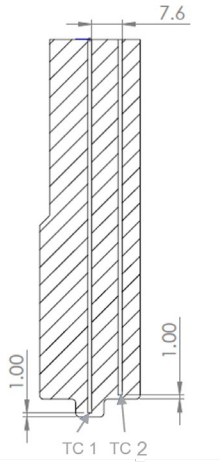

(b)

Figure S1: a) Test plate for plunging experiment, highlighting location and numbering of thermocouples, as well as where the tool will plunge. All distances in mm. b) Tool dimensions showing location of thermocouples. All measurements in mm.

S1.2 FSW Plunge Model

Material flow stresses and some material properties are provided by JMat-Pro [4] for AA 6061-T6. The temperature dependent material properties from Fig. S2 and the mechanical properties from Table S2 are used in the model. The nominal composition for AA6061-T6 is magnesium 0.8-1.2, silicon 0.4-0.8, copper 0.15-0.4, iron 0-0.7, chromium 0.04-0.35, zinc 0-0.25, and titanium 0-0.15 (in wt.%). The material properties for H13 steel are ρ = 7850 kg m^{-3}, c_p = 460 J kg^{-1} K^{-1}, and k = 24.3 W m^{-1} K^{-1}.

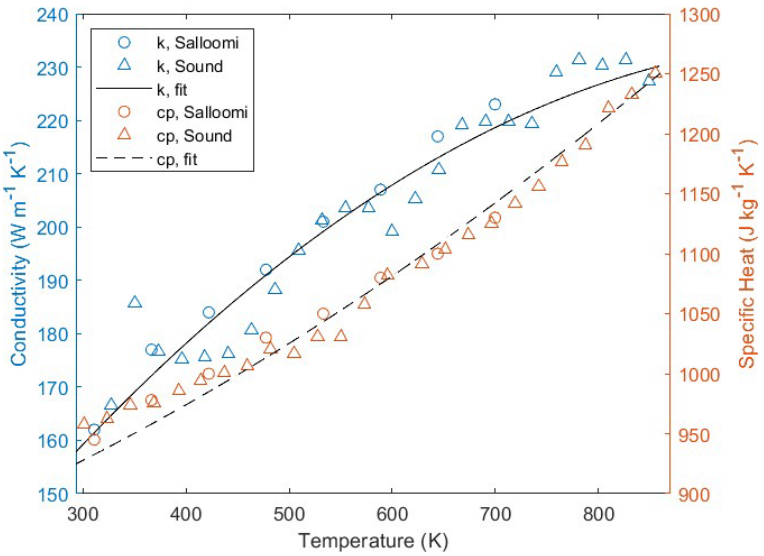

Figure S2: AA 6061-T6 thermal conductivity and specific heat as a function of temperature, from [1], [2].

Table S2: Tensile properties of AA 6061-T6

Yield Strength, MPa	Ultimate Tensile Strength, MPa	Total Elongation, %
276	27	400

The finite element discretization is based on an enhanced (P1 +/P1) 4-node tetrahedron element, as shown in Fig. S3. Temperatures are also interpolated using a piecewise linear function. The tool and workpiece meshes are shown in Fig. S4, where refinement was used in areas where large thermal and deformation gradients were expected, and elsewhere larger elements were employed to reduce computation time.

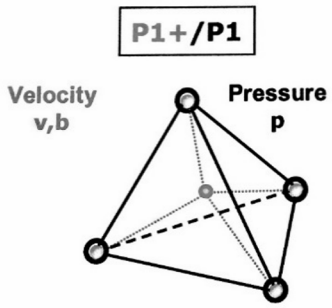

Figure S3: The P1+/P1 element is piecewise linear in both velocity and pressure, enriched by a bubble function, b, which is interpolated over the four sub-tetrahedra defined by the centroid and the four vertices, ensuring the numerical stability of the element [3].

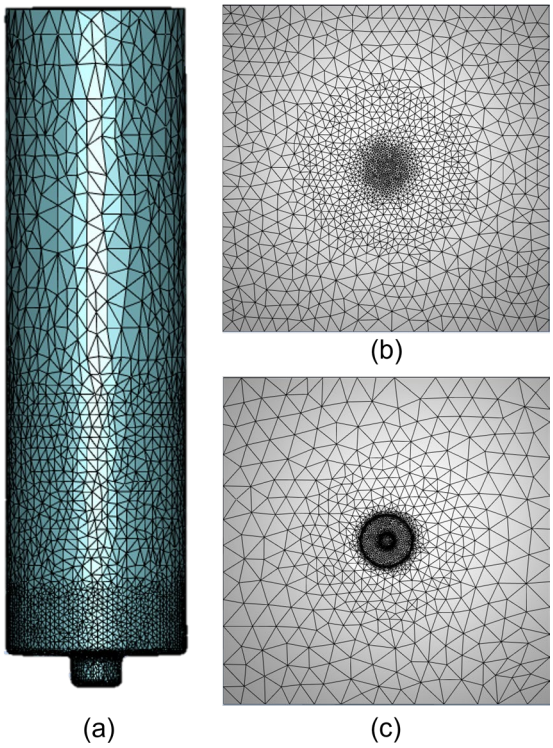

Figure S4: (a) Tool mesh. (b) Mesh for the workpiece before the simulation. (c) Mesh for the workpiece after the simulation runs to show the mesh refinement stays intact during the deformation of the simulation.

S1.3 Model Justification

To determine the validity of the simplifications, a transient heat transfer analysis based on tool properties, tool length, and length of the experiment will be discussed. The tool holder in the experiment surrounded the tool, leaving 29 mm from the shoulder of the tool exposed. The plunge lasted 20 seconds, as measured by the TCs. To determine if the tool could be treated as a semi-infinite medium for heat transfer, the Fourier number is calculated to determine if it is sufficiently low ($Fo = \frac{\alpha_{th} t}{L^2} < 0.2$ [5], where a_{th} is the thermal diffusivity of the tool, t is time, and L is the length of the exposed portion of the tool). The calculated Fo equals 0.16, which indicates that a semi-infinite assumption is valid, the heat transfer in the tool is not affected by the boundary condition between the tool and tool holder. This means that the heat generated at the tool/workpiece interface during the time of the experiment should not conduct to where the tool holder would start to affect the heat transfer. For longer experiments, the model should be modified to include the holder extending down the tool and a non-adiabatic condition should be imposed between them.

S2 Analysis/Results

The process of tuning the model consists of adjusting the friction coefficient, a, which is often modeled as a constant for the entire duration of a simulation. In the current study, the approach is to vary the friction coefficient as a function of time in order to better match the temperature profiles from the experiments. Chiumenti states that the friction coefficient is a non-linear function of the temperature and relative slip velocity making calibration difficult [6]. Fig. S5 shows how the friction coefficient was chosen to vary with time following an s-curve approach, as seen in prior work [7]. This friction curve is generated using an error function centered on the average of the maximum friction coefficient, before 7 seconds, and the minimum, after 11 seconds. The coefficient changes as the shoulder of the tool contacts the workpiece at around 7 seconds. Using a constant friction coefficient results in either extreme temperature values after the shoulder has plunged into the workpiece with mismatching slopes or inadequate heat generation and much lower temperatures for all times at the sensor locations. Thus, a greater coefficient that transitions to a lower value as the shoulder contacts

the workpiece results in the best matching of the experimental temperature profiles. As the temperature of the aluminum workpiece increases, properties like the yield strength and Young's modulus drop to about 25% of their room temperature values [1]. As a result, less friction occurs between the tool and workpiece as the temperature increases because the local shear stress that must be overcome to rotate the tool decreases. For the entire process of tuning, the heat transfer coefficient, $h_{W/T}$, was kept constant at 40 kW m^{-2} K^{-1}.

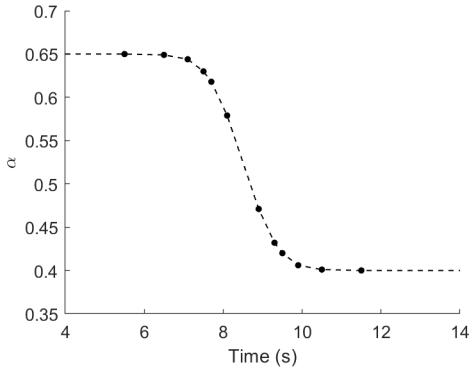

Figure S5: Linear interpolation between the points shown above was used to define the values of a with respect to time. A sufficient number of points were chosen to represent the s-curve.

An iterative approach is adopted for tuning of the friction coefficient. The specific friction law used for tuning is Norton's viscoplastic law. In this law, a is the coefficient of friction and the value that is tuned in the simulations. The initial and final values of a are subjected to the iterative tuning process, as the values that make up the curve between are auto generated using an error function, as discussed above. In addition to effects on the slope, a high initial value would cause the simulation temperatures to exceed the experimental values regardless of the final a value. For a fixed friction coefficient, matching the experiment during the first 7 seconds resulted in higher temperatures during and after the shoulder plunged into the workpiece. This is why the s-curve begins as the shoulder contacts the workpiece around 7 seconds. After tuning, the initial a value is 0.65 and the final value was 0.4, see Fig. S5 for intermediate values.

Numerical sensors are defined in the simulation workpiece at the same

locations as thermocouples in the experimental workpiece. Due to the workpiece hole tolerances where the thermocouples are located in the experiments, there is a possibility that a thermocouple could move from the center of the hole. To account for this possible source of error, the thermocouple width is measured and compared with the hole diameter to determine the possible variation in thermocouple position. Numerical sensors are introduced into the simulation at the center location as well as at distances that are possible within the hole dimensions where the thermocouple is placed. This accounts for some possible error in thermocouple positioning for the purpose of achieving a temperature match with the experiments, and is done because temperature gradients are very high in these areas of the workpiece for a short duration plunge experiment. Fig. S6 illustrates this point with a diagram of a thermocouple position in the workpiece. A match is achieved when the simulation results show similar values and slopes for temperature versus time plots when compared against the experimental values. Matching of the workpiece thermocouple temperatures is done with $h_{W/T}$ = 40 kW m^{-2} K^{-1} and a time dependent friction coefficient. Salloomi showed that a varying friction coefficient accounts for a changing sticking/slipping condition that exists between the tool and workpiece as temperature increases [1]. All other parameters match those listed in Section 2.2.1.

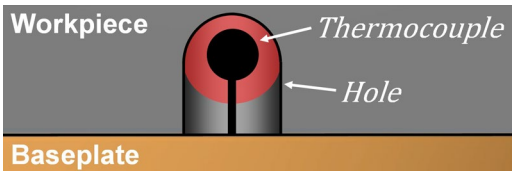

Figure S6: Schematic of the relative sizes of the thermocouple sensor and the hole for positioning the sensor in the workpiece. The red area represents the possible error in positioning caused by the difference between hole diameter and width of the thermocouple sensor. A ceramic collar below the bead is used to secure the sensor with super glue but some error in positioning could still be possible.

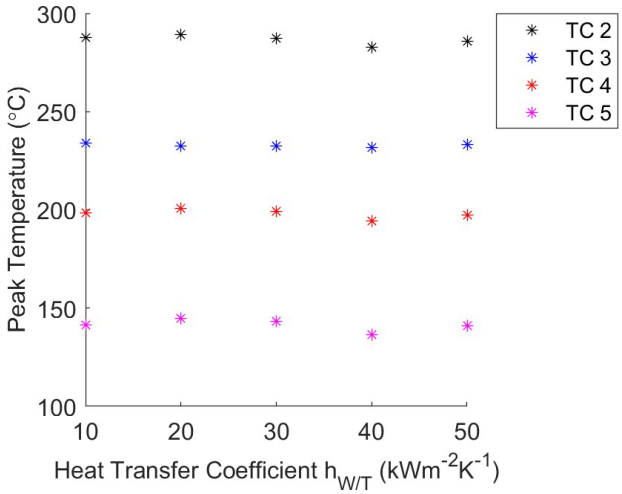

Figure S7: Plot of the simulated peak temperatures of each thermocouple for each value of $h_{W/T}$. There is no significant change between peak temperatures as $h_{W/T}$ changes.

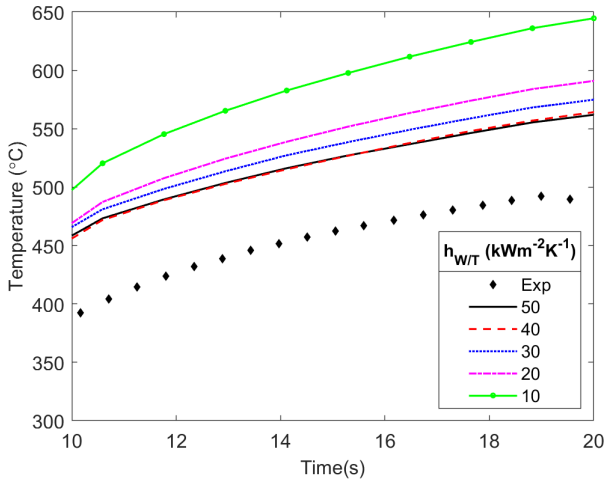

Figure S8: A zoomed in view of Figure 7 to show more clearly the spread of tool temperature with changing $h_{W/T}$.

S3 Discussion

Another previously mentioned limitation of the model is the boundary condition of the tool holder. For the 20 second plunge, the adiabatic boundary condition at the top of the tool does not materially affect the heat transfer within the tool. This is because the heat generated at the tool/workpiece interface does not have sufficient time to conduct through the tool to the holder. However, for a simulation longer than 20 seconds, the tool/holder boundary condition should play a role in the heat transfer because when $Fo > 0.2$, the tool can no longer be treated as semi-infinite. Also, the simple model geometry of the holder would need to be changed from what is shown in Fig. 5 to better match the FSW machine tool holder shown in Fig. 3. Using a more complete boundary on the tool shank could result in a marginal improvement in the current results.

A clear limitation of this model and all FSW models is that the friction coefficient is a fitting parameter. To simulate other tool geometries, process parameters, or materials, a new fit for the friction coefficient would need to be done for each case, coupled with selecting an appropriate heat transfer coefficient. Future work focused on experimentally measuring the $h_{W/T}$ coefficient would decouple the friction coefficient and heat transfer, enabling the independent tuning of frictional parameters within models. But the current results show that an S-shaped curve for the friction coefficient (Fig. S5), as a function of time, is helpful in tuning the interface heat generation to predict the experimental temperatures in workpiece and tool.

References

[1] Salloomi KN. Fully coupled thermomechanical simulation of friction stir welding of aluminum 6061-T6 alloy T-joint. Journal of Manufacturing Processes. 2019 5;45:746-54.

[2] Soundararajan V, Zekovic S, Kovacevic R. Thermo-mechanical model with adaptive boundary conditions for friction stir welding of Al 6061. International Journal of Machine Tools and Manufacture. 2005 3;45:1577-87.

[3] Pichelin E, Coupez T. Finite element solution of the 3D mold filling problem for viscous incompressible fluid. Computer Methods in Applied Mechanics and Engineering. 1998;163:359-71.

[4] Ltd SS. JMatPro; 2014.

[5] Bergman TL, Lavine AS, Incropera FP, Dewitt DP. Fundamentals of Heat and Mass Transfer. John Wiley & Sons; 2011.

[6] Chiumenti M, Cervera M, de Saracibar CA, Dialami N. Numerical modeling of friction stir welding processes. Computer Methods in Applied Mechanics and Engineering. 2013 1;254:353-69.

[7] Meyghani B, Awang M, Emamian S, Khalid NM. Developing a Finite Element Model for Thermal Analysis of Friction Stir Welding by Calculating Temperature Dependent Friction Coefficient. Springer; 2017. p. 107-26.